# Meta Distribution Characterization by Meta Statistics and Amorphous Modeling

Sara Hadavi, *Student Member, IEEE*, and Martin Haenggi, *Fellow, IEEE*

***Abstract*—In wireless network analysis, the standard signal-to-interference ratio (SIR) distribution does not capture per-link performance. The meta distribution (MD) of the SIR addresses this limitation by separating the sources of randomness, such as fading and point processes. While the MD provides a more detailed performance characterization, its computation typically depends on moments that are often difficult to obtain. Although simplified models exist that approximate MDs by ignoring parts of the interference, a structured modeling framework is needed to systematically approximate MDs according to specific accuracy and computational requirements. To address these challenges, this paper proposes a family of amorphous models, classified into three types, ordered by increasing accuracy and computational cost, to approximate the MD. We provide a comprehensive analysis of each amorphous model type in cellular and bipolar network models, identifying the scenarios where each is most suitable and the information lost in each model type. In addition, we introduce meta statistics (integral mean, integral variance, and Wasserstein variance), which capture the impact of different random elements of the network model. Finally, we analyze these meta statistics across different network models and parameters, such as fading severity and path loss exponent, for the proposed family of amorphous models.**

***Index Terms*—Meta distribution, stochastic geometry, Poisson point process, lattice, interference, signal fraction.**

## I. INTRODUCTION

### A. Motivation

In wireless networks, optimizing network performance requires mitigating interference and ensuring reliable signal quality. Stochastic geometry provides the mathematical framework to analyze wireless networks with randomly located nodes. The focus is often on the success probability $p_{\mathrm{s}}(\theta) \triangleq \mathbb{P}(\mathrm{SIR} > \theta)$ of transmissions over the typical link, which corresponds to the complementary cumulative distribution function (ccdf) of the signal-to-interference ratio (SIR).

Although this is an important performance metric, it has limited expressiveness as it obfuscates the impact of individual sources of randomness by jointly averaging over channel fading and the point process. Additionally, it quantifies the overall performance of the network and does not reveal how link reliabilities vary around $p_{\mathrm{s}}$.

To address these limitations, [1], [2], and [3] introduced the concept of meta distributions (MDs). MDs are distributions of conditional ccdfs (cccdfs) that enable the analysis of the impact of different sources of randomness separately and capture the disparity in performance of individual links in networks modeled by stationary point processes.

The authors are with The Department of Electrical Engineering, University of Notre Dame, Notre Dame, IN 46556, USA (e-mail: shadavi@nd.edu; mhaenggi@nd.edu).

The calculation of MDs is challenging since usually only the moments of the underlying distribution can be computed. Several methods exist to approximate SIR MDs, each with its own advantages and drawbacks. The standard approach to assess the accuracy of these methods is to compare the differences in MD values at each SIR threshold and reliability level. Given the importance of MDs, there is a need for models that reduce the computational complexity of SIR MDs while maintaining tractability and improving accuracy compared to existing methods, and that provide a systematic approximation framework allowing accuracy–complexity trade-offs. In addition, comparing entire MDs across different networks is often not informative for clearly identifying which networks offer better performance or for explaining the differences induced by the underlying sources of randomness. Therefore, new statistics are needed to separately capture the effects of fading and the point process, and for interpreting and comparing MDs across different networks and models.

### B. Related Work

For simplified models, where only the nearest interferer is considered, [2] and [3] provide closed-form expressions for MDs. While these models may not provide accurate approximations for more complete models, they may be used as bounds and accurately reflect their asymptotic behavior.

Most existing studies focus on networks with an infinite number of interferers, where obtaining exact closed-form expressions for MDs seems impossible. To address this, various approximation techniques based on moment methods have been proposed. The general problem of finding distributions (with bounded support) from their moments is discussed in [4]. The beta approximation, introduced in [1], estimates the MD using only the first two moments of the underlying cccdfs. A more accurate reconstruction based on all available moments is proposed in [5]. In [6], the authors employ a Fourier–Jacobi expansion to reconstruct the MD from its moments. Numerical methods for computing the MD are also presented in [6] and [7]. The beta approximation is further applied in [8] to analyze the SIR MD in multi-tier heterogeneous networks, and in [9] for the SIR MD of cell-center and cell-edge users. In [10], the negative moments of the underlying cccdfs under an inhomogeneous double-thinning approximation are obtained, and the MD is then approximated via a bounded-error Euler-sum inversion of these moments. In [11], the authors derive closed-form expressions for the moments of the underlying cccdfs by projecting a 2D $K$-tier heterogeneous network modeled by the Poisson cluster process (PCP) and the

Poisson point process (PPP) into a single-tier network on $\mathbb{R}^+$ using the mapping theorem [12]. The beta approximation is then applied to estimate the MD.

While these methods provide reasonable approximations, they rely on computing the moments of the underlying cccdfs, which itself may be difficult, and the MDs can be quite sensitive to inaccuracies in the moments [13].

In [14], the concept of *simalysis* is introduced, in which interference from nodes within a certain distance is simulated, while interference from nodes beyond that distance is approximated by its analytical mean. This technique improves computational efficiency and enhances accuracy, particularly as the path loss exponent decreases to 2, where interference from distant nodes dominates the total interference.

Based on the same idea, [15] proposes the dominant interferer approximation, where the first $j$ nearest interferers are modeled exactly, while the remaining interference is approximated by its analytical mean. The authors analyzed the nearest interferer (dominant) case and demonstrated that this approach closely matches the beta approximation and, in some cases, outperforms it. While this model reduces computational complexity and enhances tractability, it does not account for the variance of the aggregate interference from non-dominant interferers, effectively ignoring the impact of fading in interference, which can be beneficial. In [16], a dominant-interferer-based approximation is further used to approximate the SIR MD in Poisson networks with dynamic traffic. This approximation enables the analysis of interacting queues by allowing transmitter activity and queue stability conditions to be expressed in terms of the conditional success probability, and is used to study spatial outage capacity under queue stability constraints. Lastly, [17] proposes a model in which the dominant interferer's effect is captured exactly and the aggregate interference from the remaining interferers is approximated by a Gaussian random variable characterized by their mean and variance.

### C. Contributions

This work focuses on meta statistics that capture essential information of the MD, including the overall network performance and the individual effects of the two sources of randomness, the point process and fading. In addition, it introduces a systematic approach to approximate the interference model by progressively increasing the model complexity and accuracy. The contributions of this paper are as follows:

- We introduce a family of amorphous models designed to simplify interference representation and analysis. These models approximate more complete representations by retaining only the dominant interferer while approximating the remaining interference using its statistics. The family has three types, called amorphous models of Type 0, 1, and 2, distinguished by the extent to which statistics of the residual interference are captured.
  Previous studies applied models of Type 0 and Type 1, respectively [3], [15]. In this paper, we introduce and analyze the Amorphous Type 2 model, together with the Type 0 and Type 1 models.
- We establish a unified framework for cellular and bipolar network models, highlighting that their only distinction is the dependence between the desired and dominant interfering link distances.
- Based on this framework, we analyze the family of amorphous models and derive general analytical expressions for the signal fraction (SF) MD [18] applicable to all point processes. The focus of this study is on PPPs and square lattices. We explore the advantages and limitations of each amorphous model and identify scenarios where each is best suited. The accuracy of each model is quantified using the total distance metric, and efficiency is assessed based on computational runtime.
- We utilize the Amorphous Type 2 model to demonstrate that fading in the interference improves the success probability and, consequently, MDs.
- We introduce three scalar meta statistics: the integral mean, the integral variance, and the Wasserstein variance, which effectively capture key features of the MDs and greatly simplify comparisons across different network models.
- We utilize the meta statistics to compare the three types of amorphous models and evaluate how closely they approximate the fully granular interference model. This comparison highlights the specific information each model type captures, as each statistic reveals distinct aspects of the MD.

In this paper, we utilize the following notations:

$$x^{\ominus} = \frac{x}{1-x}, \quad x \in \mathbb{R} \setminus \{1\},$$

$$x^{\oplus} = \frac{x}{1+x}, \quad x \in \mathbb{R} \setminus \{-1\},$$

$I(x; a, b)$ is the regularized incomplete beta function, and $B(a, b)$ is the beta function.

The remainder of this paper is organized as follows. In Section II, we review MDs and introduce three scalar meta statistics, along with their fundamental properties and illustrative examples based on the nearest-interferer-only model. In Section III, we introduce the family of amorphous models alongside the fully granular model and describe how the former approximates the latter. Section IV employs this family to approximate the MDs and derives integral expressions for the corresponding approximations. In Sections V and VI, the MD expressions obtained in Section IV are specialized to cellular and bipolar network models, respectively, considering both Poisson point processes and square lattices.

## II. Meta Statistics in Wireless Networks

### A. Definition of the MD

We refer to nonnegative random variables (RVs), such as the SIR, that characterize the user experience as *performance random variables* (PRVs) [5], distinguishing them from *performance metrics*, which are deterministic quantities. The PRVs depend on two sources of randomness, namely the point process and fading. The distribution of PRVs is commonly used to assess wireless network performance. However, due to the nature of wireless networks, the PRVs strongly depend on the user's location and are also time-varying. To analyze these effects separately, we consider MDs, which are the distributions of cccdfs conditioned on the point process of transceiver locations. The cccdfs are given by

$$P_t \triangleq \mathbb{P}(Z > t \mid \Phi), \quad t \in \mathbb{R}, \tag{1}$$

where $Z$ is the PRV and $\Phi$ is the point process. Since the conditional probability measure accounts for random fading while conditioning on the point process, MDs dissect spatial and temporal randomness in the network model [2]. The MD is the ccdf of $P_t$, i.e.,

$$\bar{F}(t,u) \triangleq \mathbb{P}(P_t > u), \quad u \in [0,1], \quad t \in \mathbb{R}, \tag{2}$$

The $(b,t)$-th moment of the MD is defined as [5]

$$M_b(t) \triangleq \mathbb{E}(P_t^b) = \int_0^1 bu^{b-1}\bar{F}(t,u)\,\mathrm{d}u. \tag{3}$$

Comparing entire MDs across different networks does not easily reveal which network performs better or explain the reasons behind the differences. To address this, we introduce three scalar statistics of MDs.

### B. Statistics of the MD

**Definition 1** (Integral Mean)**.** *The integral mean represents the volume under the surface of the MD and is the mean of the PRV. It is given by*

$$\mathcal{M} \triangleq \mathbb{E}(Z) = \int_0^\infty M_1(t)\,\mathrm{d}t = \int_0^\infty \int_0^1 \bar{F}(t,u)\,\mathrm{d}u\,\mathrm{d}t. \tag{4}$$

**Definition 2** (Integral Variance)**.** *The integral variance $\mathcal{V}$ is defined as*

$$\mathcal{V} \triangleq \int_0^\infty \mathrm{Var}(P_t)\ \mathrm{d}t = \int_0^\infty (M_2(t) - M_1(t)^2)\mathrm{d}t. \tag{5}$$

$\mathcal{V}$ aggregates the variability of the conditional success probability $P_t$ over all PRV thresholds and measures how strongly the network performance depends on the point process.

**Definition 3** (Wasserstein Variance)**.** *The Wasserstein variance $\mathcal{W}$ is defined as*

$$\mathcal{W} \triangleq \int_0^\infty \int_0^1 |\bar{F}(t,u) - M_1(t)|\mathrm{d}u\,\mathrm{d}t. \tag{6}$$

$\mathcal{W}$ measures the deviation of the MD from the success probability $M_1(t) = \mathbb{P}(Z > t)$. As shown later, without fading $\mathcal{W} = 0$, and, as the severity of the fading increases, $\mathcal{W}$ approaches a finite supremum value. $\mathcal{W}$ is upper bounded as follows if the PRV has finite support.

**Proposition 1.** *If the PRV is supported on $[q_1, q_2]$,*

$$\mathcal{W} \le \frac{q_2 - q_1}{2}.$$

*Proof:* For every $t$, the function $\bar{F}(t,u)$ maps $[0,1]$ to $[0,1]$ with a mean $M_1(t)$. The integral

$$V = \int_0^1 |\bar{F}(t,u) - M_1(t)|\,\mathrm{d}u,$$

is maximized when $\bar{F}(t,u)$ deviates from its mean as much as possible, which occurs if it takes values 0 or 1 over two disjoint sub-intervals. Let

$$\bar{F}(t,u) = \begin{cases} 1, & 0 \le u < a, \\ 0, & a \le u \le 1, \end{cases}$$

for some $a \in [0,1]$. This results in $m_1(t) = a$, and

$$V = 2a(1-a),$$

which is maximized at $a = 1/2$, yielding $V \le 1/2$. Thus,

$$\mathcal{W} = \int_{q_1}^{q_2} V\,dt \le \int_{q_1}^{q_2} \frac{1}{2}\,dt = \frac{q_2 - q_1}{2}.$$

■

To highlight the characteristics of the integral variance and the Wasserstein variance, we consider different distinct scenarios based on whether the two sources of randomness, point process and fading, are considered deterministic (D) or random (R).

**Proposition 2.** *In the case where both sources of randomness are present (RR), $\mathcal{W} > 0$, and $\mathcal{V} > 0$.*

*Proof:* Due to the the point process, $P_t$ is random, i.e., $\mathrm{Var}(P_t) > 0$, and therefore $\mathcal{V} > 0$. Also, since $Z$ is a non-degenerate RV, $P_t \in (0,1)$ on a set of positive measure. This ensures that $\bar{F}(t,u)$ is strictly decreasing in $u$ and therefore, $\bar{F}(t,u) \neq M_1(t)$. As a result, $\mathcal{W} > 0$. ■

**Proposition 3.** *For $\Phi = \varphi$, i.e., for a realization of the point process, and random fading (DR), the MD satisfies $\bar{F}(t,u) \in \{0,1\}$, resulting in $\mathcal{V} = 0$ and $\mathcal{W} > 0$.*

*Proof:* The conditional success probability

$$P_t = \mathbb{P}(Z > t \mid \Phi = \varphi)$$

is deterministic as a function of $\varphi$. Thus, the MD of the PRV simplifies to

$$\bar{F}(t,u) = \mathbb{P}(P_t > u) = \mathbf{1}\ (P_t > u), \tag{7}$$

which results in $M_b(t) = P_t^b$. It follows that

$$\mathcal{V} = \int_0^\infty (P_t^2 - P_t^2)\,\mathrm{d}t = 0,$$

$$\mathcal{W} = \int_0^\infty \left[\int_0^{P_t} (1 - P_t)\,du + \int_{P_t}^1 P_t\,du\right] dt$$
$$= \int_0^\infty 2P_t(1 - P_t)\,dt.$$

Due to fading, $P_t \in (0,1)$ on a set of positive measure. Thus, $\mathcal{W} > 0$. ■

**Proposition 4.** *Without fading (RD), the MD of the PRV does not depend on $u$, resulting in $\mathcal{W} = 0$ and $\mathcal{V} > 0$.*

*Proof:* Without fading, the cccdf simplifies to

$$P_t = \mathbf{1}(Z > t \mid \Phi). \tag{8}$$

The MD of the PRV is

TABLE I
SUMMARY OF RANDOMNESS AND RESULTING VARIANCES IN META STATISTICS. $h_i$ IS THE FADING COEFFICIENT.

| Scenario | Random elements | $\mathcal{V}, \mathcal{W}$ |
|---|---|---|
| Random-Random (RR) | $\Phi,\ h_i$ | $\mathcal{V} > 0,\ \mathcal{W} > 0$ |
| Deterministic-Random (DR) | $h_i$ | $\mathcal{V} = 0,\ \mathcal{W} > 0$ |
| Random-Deterministic (RD) | $\Phi$ | $\mathcal{V} > 0,\ \mathcal{W} = 0$ |
| Deterministic-Deterministic (DD) | none | $\mathcal{V} = 0,\ \mathcal{W} = 0$ |

$$\bar{F}(t,u) = \mathbb{P}(P_t = 1) = \mathbb{P}(Z > t), \tag{9}$$

which does not depend on $u$. Since $M_b(t) = \mathbb{P}(Z > t)$, it follows that

$$\mathcal{W} = \int_0^\infty \int_0^1 |\bar{F}(t,u) - M_1(t)| \, \mathrm{d}u \, \mathrm{d}t = 0,$$

and

$$\mathcal{V} = \int_0^\infty \mathbb{P}(Z > t)(1 - \mathbb{P}(Z > t)) \, \mathrm{d}t.$$

Due to the point process, $\mathbb{P}(Z > t) \in (0,1)$ on a set of positive measure. Thus, $\mathcal{V} > 0$. ∎

**Corollary 1.** *Without any randomness (DD), the MD of the PRV does not depend on $u$ and satisfies $\bar{F}(t,u) \in \{0,1\}$, resulting in $\mathcal{W} = \mathcal{V} = 0$.*

*Proof:* The result follows by combining Propositions 3 and 4. ∎

The above propositions highlight how $\mathcal{V}$ and $\mathcal{W}$ are sensitive to different random elements of the network model. The integral variance measures the spread in the MD due to the spatial randomness of the point process and increases with greater clustering. The Wasserstein variance measures the disparity in the MD caused by fading and increases as the variance of the fading increases. A summary of Propositions 2 to 4 and Cor. 1 is provided in Table I.

A particularly important PRV is the SIR, defined as $\mathrm{SIR} \triangleq S/I \in [0,\infty)$, where $S$ is the signal power and $I$ is the interference power. Since the SIR may be unbounded, its complete distribution cannot be visualized. In contrast, the signal fraction (SF), defined as $\mathrm{SF} \triangleq S/(S+I)$, is supported on $[0,1]$ [18]; thus, all its positive moments always exist, and no truncation is needed when visualizing its distribution. Moreover, the bounded support and range of SF MDs make it easy to compare the gap between different approximations of SF MDs. For these reasons, we focus on the SF. The conditional success probability is defined as the cccdf of SF, given by

$$P_t \triangleq \mathbb{P}(\mathrm{SF} > t \mid \Phi), \quad t \in [0,1], \tag{10}$$

and the SF MD is given in (2).

To illustrate the results in Propositions 1 to 4 and Cor. 1, we consider the nearest interferer-only model for the SF MD.

### C. Nearest Interferer-Only Model

Consider a downlink cellular network where base stations (BSs) are distributed according to a stationary point process $\Phi \subset \mathbb{R}^2$ with nearest-BS association and Nakagami-$m$ fading. If only the nearest interferer is considered, the SF is given by

$$\mathrm{SF} = \frac{h_0 r_0^{-\alpha}}{h_0 r_0^{-\alpha} + h_1 r_1^{-\alpha}},$$

where $h_k$ are the fading RVs, $r_0$ and $r_1$ are the distances to the serving and nearest interfering BS, respectively, and $\alpha$ is the path loss exponent. The SF MD for the RR scenario is [3]

$$\bar{F}(t,u) = \min\left\{1, \left(\frac{q(u)^{\ominus}}{t^{\ominus}}\right)^{\delta}\right\}, \tag{11}$$

where $\delta \triangleq 2/\alpha$, and $q(u) \triangleq I^{-1}(1-u; m, m)$ is the inverse of the regularized incomplete beta function. The three statistics of the SF MD can be obtained using (3) to (6) by numerical integration. From Fig. 1a, we observe that SF MD varies smoothly, depending on both $u$ and $t$, indicating the presence of both sources of randomness. The contour plot in Fig. 1b shows a smooth transition of contour lines from 1 (highest SF MD) to 0 (lowest SF MD) and a gradual decrease in reliability as the SF threshold increases along each line. The expressions for the SF MD, its $(b,t)$-th moment, and its statistical metrics for the DR, RD, and DD scenarios are provided in Tables IIa, IIb, and IIc, respectively, and proofs of the expressions presented in these tables are provided in Appendices A, B, and C, respectively. In the tables, $\rho = (r_2/r_1)^\alpha$, and $\bar{G}(t) = 1 - I(t/(t(1-\rho)+\rho); m, m)$ is the ccdf of the SF.

For the DR scenario from Fig. 1c, we observe that SF MD is either 1 or 0 and depends on both $u$ and $t$, indicating that fading is the only source of randomness. Additionally, the contour plot in Fig. 1d shows all contour lines collapsing onto

TABLE II
EXPRESSIONS FOR THE DR, RD, AND DD SCENARIOS.

**(a) DR**

| Metric | Expression |
|---|---|
| **SF MD** | $\bar{F}(t,u) = \mathbf{1}\{\bar{G}(t) > u\}$ |
| **$(b,t)$-th moment** | $M_b^{\mathrm{DR}}(t) = \bar{G}(t)^b$ |
| **Integral mean** | $\mathcal{M}^{\mathrm{DR}} = \int_0^1 \bar{G}(t)\,\mathrm{d}t$ |
| **Integral variance** | $\mathcal{V}^{\mathrm{DR}} = 0$ |
| **Wasserstein variance** | $\mathcal{W}^{\mathrm{DR}} = \int_0^1 2\bar{G}(t)[1-\bar{G}(t)]\,\mathrm{d}t$ |

**(b) RD**

| Metric | Expression |
|---|---|
| **SF MD** | $\bar{F}(t,u) = \min\{1, (t^{\ominus})^{-\delta}\}$ |
| **$(b,t)$-th moment** | $M_b^{\mathrm{RD}}(t) = \min\{1, (t^{\ominus})^{-\delta}\}$ |
| **Integral mean** | $\mathcal{M}^{\mathrm{RD}} = \frac{1}{2} + \frac{1}{\mathrm{sinc}(\delta)} - B_{1/2}(1-\delta, \delta+1)$ |
| | $\mathcal{M}^{\mathrm{RD}} = \frac{\pi}{4},\ \delta = \frac{1}{2}$ |
| **Integral variance** | $\mathcal{V}^{\mathrm{RD}} = \frac{1}{\mathrm{sinc}(\delta)} - \frac{1}{\mathrm{sinc}(2\delta)} + C,\ \delta \in (0,1) \setminus \{\frac{1}{2}\}$ |
| | $C = B_{1/2}(1-\delta, \delta+1) - B_{1/2}(1-2\delta, 2\delta+1)$ |
| | $\mathcal{V}^{\mathrm{RD}} = 0.09227,\ \delta = \frac{1}{2}$ |
| **Wasserstein variance** | $\mathcal{W}^{\mathrm{RD}} = 0$ |

**(c) DD**

| Metric | Expression |
|---|---|
| **SF MD** | $\bar{F}(t,u) = \mathbf{1}\{\rho^{\oplus} > t\}$ |
| **$(b,t)$-th moment** | $M_b^{\mathrm{DD}}(t) = \mathbf{1}\{\rho^{\oplus} > t\}$ |
| **Integral mean** | $\mathcal{M}^{\mathrm{DD}} = \rho^{\oplus}$ |
| **Integral variance** | $\mathcal{V}^{\mathrm{DD}} = 0$ |
| **Wasserstein variance** | $\mathcal{W}^{\mathrm{DD}} = 0$ |

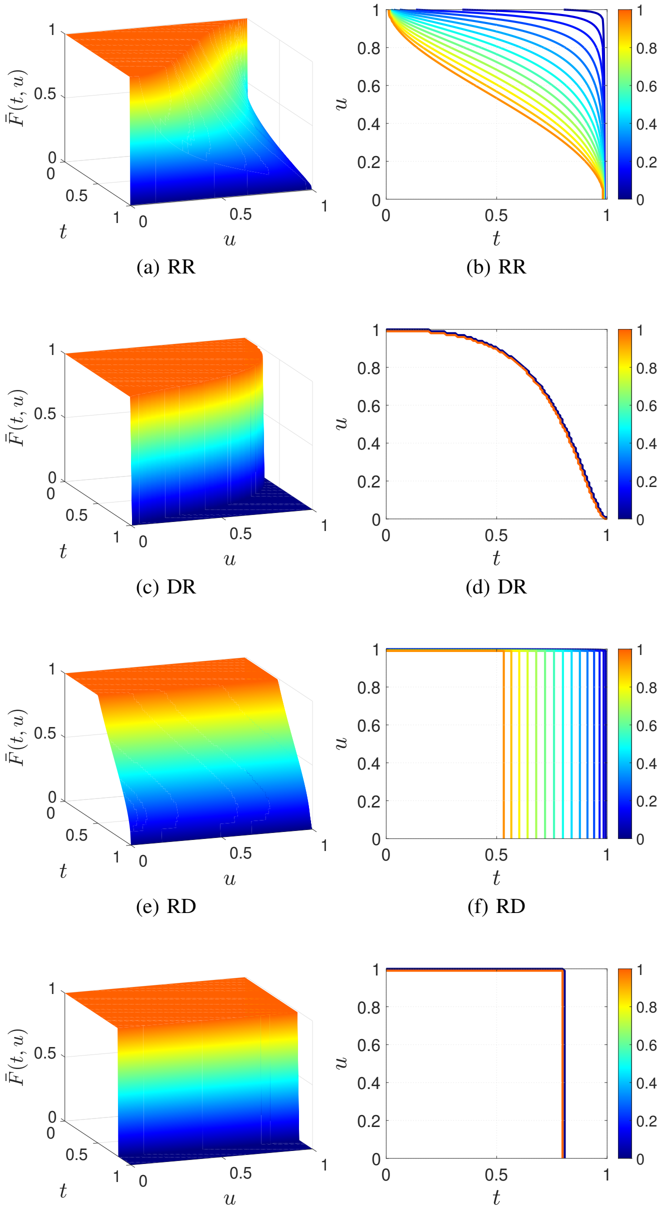

(a) RR (b) RR

(c) DR (d) DR

(e) RD (f) RD

(g) DD (h) DD

Fig. 1. Left: Three-dimensional plots of the SF MD. Right: Corresponding contour plots of SF MD, for $\alpha = 4$. For the RR and DR scenarios, $m = 2$.

each other, indicating that SF MD takes only the values 0 or 1. It also highlights the transition point, which can be determined from $M_1(t)$ for each $t$.

For the RD scenario from Fig. 1e, we observe that the SF MD varies smoothly and remains constant along the $u$ axis, indicating there is no fading. Additionally, the contour plot in Fig. 1f shows contour lines gradually decreasing from 1 to 0 and are parallel to the $u$ axis.

For the DD scenario, Fig. 1g illustrates that the SF MD remains constant along the $u$-axis and is either 1 or 0, which indicates there is no source of randomness. From Fig. 1h, we observe that all contour lines collapse onto each other, indicating that SF MD takes only 1 or 0 and that the transition occurs at the same SF threshold for all reliability levels.

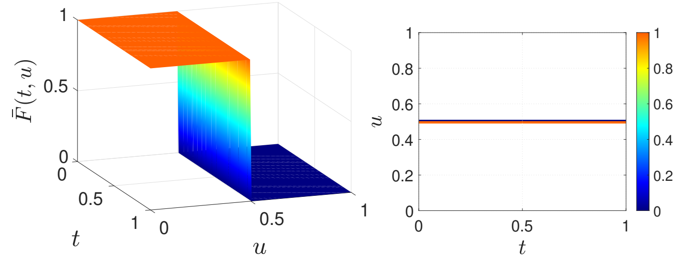

(a) RR (b) RR

Fig. 2. Left: Three-dimensional plot of the SF MD. Right: Corresponding contour plot of SF MD, for $\alpha = 4$ and extreme fading.

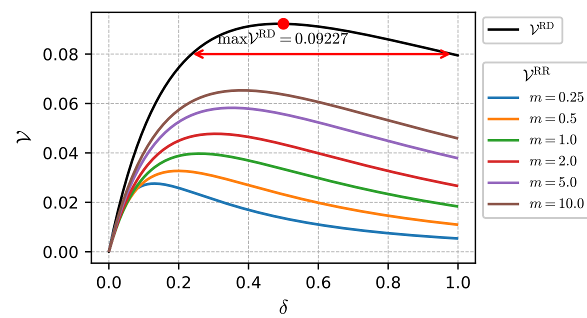

Fig. 3. Dependence of $\mathcal{V}$ on $\delta$, showing insensitivity of $\mathcal{V}$ to $\delta$ for the SF MD, under DR and RR scenarios.

For the SF MD, by Proposition 1, $\mathcal{W} \leq 1/2$. As illustrated in Fig. 2, under extreme fading, i.e., when the fading variance goes to infinity, $\bar{F}(t,u) \in \{0,1\}$, which results in the maximum deviation from its mean and corresponds to $\mathcal{W} = 1/2$. In this case, the SF MD does not depend on $t$. Conversely, without fading, the SF MD does not depend on $u$. Together with Proposition 4, which corresponds to the no fading case where $\mathcal{W}$ attains its minimum, this shows that the Wasserstein variance measures the severity of the fading effects in the network.

*Remark:* For the RD scenario, from Fig. 3, we observe $\mathcal{V}^{\mathrm{RD}}$ as a function of $\delta$. As indicated by the red double-headed arrow, for most values of $\delta$, $\mathcal{V}^{\mathrm{RD}} \in [0.08, 0.09227]$, showing that the integral variance is insensitive to $\delta$. $\mathcal{V}^{\mathrm{RR}}$ varies even less with $\delta$. This behavior is notable, as many performance metrics in wireless networks strongly depend on the path loss exponent, such as $M_b(t)$. However, $M_2(t)$ and $M_1(t)^2$ exhibit similar trends with respect to $\delta$ and are close over most of the SF threshold range, with a moderate difference emerging only at high thresholds as $m$ increases. Thus, their difference, which determines $\mathcal{V}$, becomes small and results in $\mathcal{V}$ being insensitive to $\delta$.

To analyze the SF MD statistics in more complete models, we introduce a family of models in the next section. These are utilized to approximate the more complete models, and we compare their statistics to determine which provides the most accurate results.

TABLE III
SUMMARY OF THE FAMILY OF AMORPHOUS MODELS

| Type | Model | Properties |
|---|---|---|
| Type 0 | $A_0$ | $\mu_X = 0$ |
| Type 1 | $A_1$ | $\mu_X > 0, H = 1$ |
| Type 2 | $A_2$ | $\mu_X > 0, \mathrm{Var}(H) > 0$ |

## III. AMORPHOUS AND FULLY GRANULAR MODELS

### A. Family of Amorphous Models

The family of amorphous models characterizes the interference as the sum of two terms,

$$I \triangleq I_{\mathrm{D}} + X, \tag{12}$$

where $I_{\mathrm{D}}$ is a RV representing the dominant interference term, and $X$ is either 0, deterministic, or another RV. We define $X$ as

$$X \triangleq H\mu_X, \tag{13}$$

where $H$ is a positive RV with $\mathbb{E}(H) = 1$, and $\mu_X = \mathbb{E}[X]$. The amorphous models are classified into three types based on the properties of $H$ and $\mu_X$.

*1) Type 0:* The Amorphous Type 0 model ($A_0$) is defined as

$$I = I_{\mathrm{D}},$$

i.e., $\mu_X = 0$, and it is the simplest model. An example of this model is the nearest interferer-only model.

*2) Type 1:* The Amorphous Type 1 model ($A_1$) extends Type 0 by incorporating a deterministic term and is defined as

$$I = I_{\mathrm{D}} + \mu_X, \tag{14}$$

where $\mu_X > 0$, i.e., $H = 1$ in (13). This model is applicable for dominant interferer-based approximations [15]. Additionally, it can be used to model the signal-to-interference-plus-noise (SINR) MD, where the noise is typically represented as white Gaussian noise with variance $\sigma^2$ [19]. By setting $\mu_X = \sigma^2$ in (14), the model accounts for the noise in the system.

*3) Type 2:* The Amorphous Type 2 model ($A_2$) extends Type 1 by incorporating variability in $H$ and is defined as

$$I = I_{\mathrm{D}} + H\mu_X, \tag{15}$$

where $\mathrm{Var}(H) > 0$ and $\mu_X > 0$.

$A_2$ is mainly used to represent a dominant interferer along with the mean and variance of the remaining interference. Another application of this model is in scenarios where two interferers are considered, such as the first and second nearest interferers or a dominant interferer along with a special interferer at a specified distance $r_{\mathrm{s}}$. A summary of the family of amorphous models is provided in Table III.

This family can be generalized to $A_3$, $A_4$,..., $A_\infty$, where the subscript indicates the number of matched central interference moments. In particular, $A_\infty$, which matches all moments, accounts for the interference exactly.

### B. Fully Granular Model and Amorphous Approximations

In contrast to the family of amorphous models, the fully granular model accounts for the complete interference without any simplification. Let $\Phi = \{x_0, x_1, x_2, \dots\} \subset \mathbb{R}^2$ be a set of transmitters where $x_0$ is the desired transmitter. In the cellular model, $\Phi$ is a stationary point process, and in the bipolar model, $\Phi \setminus \{x_0\}$ forms a stationary point process with $x_0$ independent of $\Phi$. We assume $x_1$ to be the strongest interferer (averaged over fading), i.e.,

$$\|x_i\| > \|x_1\|, \quad i > 1$$

and define

$$r_i \triangleq \|x_i\|.$$

The signal power is given by $S = h_0 r_0^{-\alpha}$. Then, the fully granular model is defined as

$$\mathring{I} \triangleq \sum_{i\in\mathbb{N}} h_i r_i^{-\alpha}. \tag{16}$$

Here, $h_i$ are independent RVs, with $\mathbb{E}[h_i] = 1$, representing fading. While this model provides an exact representation of the interference, the infinite sum makes it computationally intractable. To resolve this, we apply amorphous modeling. We first express (16) as

$$\mathring{I} = I_{\mathrm{D}} + I', \tag{17}$$

where

$$I_{\mathrm{D}} = h_1 r_1^{-\alpha}, \tag{18}$$

and

$$I' = \sum_{i\in\mathbb{N}\setminus\{1\}} h_i r_i^{-\alpha}. \tag{19}$$

The family of amorphous models approximates the fully granular model (17) with different levels of accuracy by retaining the dominant interferer effect $I_{\mathrm{D}}$, and approximating $I'$ by a RV $X$ that, like $I_{\mathrm{D}}$, depends on $r_1$.

For any stationary point process with density $\lambda$, the mean interference from the nodes outside a distance $c$ is [14]

$$J(c) = \mathbb{E}\sum_{i\in\mathbb{N}\setminus\{1\}} r_i^{-\alpha} = 2\pi\lambda\int_c^\infty r^{1-\alpha}\,\mathrm{d}r = \frac{2\pi\lambda}{\alpha-2}c^{2-\alpha}. \tag{20}$$

Thus, the mean of $I'$ given $r_1$ is

$$\mu_X = J(r_1) = \frac{2\pi\lambda}{\alpha-2}\, r_1^{2-\alpha}.$$

Depending on the type of amorphous model, $X$ approximates $I'$ either by zero, by its mean, or by matching both its mean and variance:

$$\mathring{I} \approx \begin{cases} I_{\mathrm{D}}, & \text{in } A_0, \\ I_{\mathrm{D}} + \mu_X, & \text{in } A_1, \\ I_{\mathrm{D}} + H\mu_X, & \text{in } A_2, \end{cases} \tag{21}$$

where

$$\mathrm{Var}(H \mid r_0, r_1) = \frac{\mathrm{Var}(X \mid r_0, r_1)}{\mu_X^2} = \frac{\mathrm{Var}(I' \mid r_0, r_1)}{\mu_X^2}. \tag{22}$$

Thus, the family of amorphous models requires the exact power of only the desired transmitter and the dominant interferer, while the interference from the remaining transmitters is captured using at most first- and second-order statistics.

Although $\mathrm{A}_0$ may not be a good approximation, it allows for closed-form expressions that serve as bounds for more complete models and accurately reflect their asymptotic behavior.

$\mathrm{A}_1$ is more accurate than $\mathrm{A}_0$ as it accounts for the mean of $I'$. $\mathrm{A}_2$ provides the best approximation among the three types of amorphous models since it accounts for both the mean and variance of $I'$, through the RV $X$.

## IV. Application to the SF MD

### A. System Model

We consider the system model in Subsec III-B, with $h_0 \sim \Gamma(m_0, m_0)$ and $h_i \sim \Gamma(m, m)$ for $i \geq 1$. For $\mathrm{A}_2$, let $X$ be a conditionally gamma RV given $r_0$ and $r_1$. Then, $H$ is also conditionally gamma distributed with mean 1 and shape parameter $M$, given by

$$M = \frac{1}{\mathrm{Var}(H \mid r_0, r_1)} = \frac{\mu_X^2}{\mathrm{Var}(X \mid r_0, r_1)}, \tag{23}$$

using (22). $M$ depends on $m$ and the point process model.

### B. SF MD for Amorphous Models

The SF is given by

$$\mathrm{SF} = \frac{S}{S + I_\mathrm{D} + I'} \tag{24}$$

and is approximated by the family of amorphous models as follows

$$\mathrm{SF} \approx \begin{cases} \mathrm{SF}_0 = \dfrac{S}{S + I_\mathrm{D}}, & \mathrm{A}_0, \\ \mathrm{SF}_1 = \dfrac{S}{S + I_\mathrm{D} + \mu_X}, & \mathrm{A}_1, \\ \mathrm{SF}_2 = \dfrac{S}{S + I_\mathrm{D} + H\mu_X}, & \mathrm{A}_2. \end{cases} \tag{25}$$

The conditional success probability under $\mathrm{A}_k$, $k = 0, 1, 2$, is

$$P_t^{(k)} = \mathbb{P}(\mathrm{SF}_k > t \mid r_0, r_1).$$

*1) Amorphous Type 0:* For $\mathrm{A}_0$, when $m_0 = m$, the SF MD is provided in (11), and for $m_0 = m = 1$, closed-form expressions are given in [3, Eq. 7] for Poisson cellular networks and [3, Eq. 10] for Poisson bipolar networks.

**Theorem 1.** *For $A_0$, in the general case where $m_0 \neq m$ and for any point process, the SF MD is given by*

$$\bar{F}(t, u) = F_R(\theta_{t,u}), \tag{26}$$

*where $R \triangleq r_0/r_1 \in (0, 1]$ is the distance ratio, $F_R$ is its cumulative distribution function (cdf), and*

$$\theta_{t,u} \triangleq \left(\frac{m\, x_u^{\ominus}}{m_0\, t^{\ominus}}\right)^{\delta/2}, \quad x_u \triangleq I^{-1}(1 - u; m_0, m).$$

*Proof:* Follows from [20, Thm. 1], where, given the geometry, the ccdf of the SIR for $m_0 \neq m$ is expressed as

$$\mathbb{P}(\mathrm{SIR} > \theta) = \mathbb{P}\left(R < \left(\frac{m\, x_u^{\ominus}}{m_0\, \theta}\right)^{\delta/2}\right).$$

with $\theta = t^{\ominus}$. Here, this result is used for the SF and generalized by averaging over the distance ratio probability density function (pdf) $f_R$ for arbitrary point processes. ■

*2) Amorphous Type 1:* For $\mathrm{A}_1$ with $m_0 = m = 1$, the integral expression of the SF MD is given in [15, Cor. 1], with corresponding expressions for various point processes provided in [15, Sec. IV].

**Lemma 1.** *For $A_1$, when $m_0 = m$, the conditional success probability can be expressed by the McKay Type II distribution [21].*

*Proof:* See Appendix D. ■

The pdf of the McKay Type II distribution is given in (66) in Appendix D.

**Theorem 2.** *For $A_1$, the SF MD for $m_0 = 1$ and $h_1 \sim \Gamma(m, m)$ is*

$$\bar{F}(t, u) = \int_0^\infty \int_0^{\zeta_{t,u}} v f_{r_0, r_1}(w, v)\, dw\, dv, \tag{27}$$

*where $\zeta_{t,u} = \sqrt{\ln((1 + t^{\ominus} r^\alpha/m)^{-m}/u)/(\kappa r^\alpha)}$, and for $m_0 = m$, the SF MD is*

$$\bar{F}(t, u) = \int_0^\infty \int_0^{\sqrt{\frac{F_{\mathrm{MK}}^{-1}(1-u)}{\kappa\, r^\alpha}}} v\, f_{r_0, r_1}(rv, v)\, \mathrm{d}v\, \mathrm{d}r, \tag{28}$$

*where $\kappa = 2\pi\lambda t^{\ominus}/(\alpha - 2)$, $r = w/v$, $f_{r_0, r_1}$ is the joint pdf of $r_0$ and $r_1$, $F_{\mathrm{MK}}$ is the cdf of the McKay Type II distribution with parameters*

$$a = m - \tfrac{1}{2}, \quad b = \frac{2}{m}(t^{\ominus} r)^{\oplus}, \quad c = 2(t^{\ominus} r)^{\oplus} - 1,$$

*and $F_{\mathrm{MK}}^{-1}$ is its quantile function.*

*Proof:* For $m_0 = 1$ and $h_1 \sim \Gamma(m, m)$, the conditional success probability is

$$\begin{aligned} P_t^1 &= \mathbb{P}\big(h_0 > t^{\ominus} r_0^\alpha \big(h_1 r_1^{-\alpha} + \mu_X\big) \big| r_0, r_1\big) \\ &= e^{-t^{\ominus} \mu_X r_0^\alpha} \left(1 + \frac{t^{\ominus}}{m}\left(\frac{r_0}{r_1}\right)^\alpha\right)^{-m} \\ &= e^{-\kappa\, t^{\ominus}\, R^\alpha r^2} \left(1 + \frac{t^{\ominus}}{m} R^\alpha\right)^{-m}, \end{aligned} \tag{29}$$

where $R = r_0/r_1$. Substituting (29) into (2) gives (27). For $m_0 = m$, the conditional success probability follows from Lemma 1 as

$$P_t = 1 - F_{\mathrm{MK}}\big(\kappa R^\alpha r_1^2\big)\,. \tag{30}$$

Substituting (30) into (2) yields

$$\bar{F}(t, u) \int_0^\infty \int_0^\infty \mathbf{1}\big(F_{\mathrm{MK}}\big(\kappa r^\alpha v^2\big) < 1 - u\big)\, f_{r_0, r_1}(w, v)\, \mathrm{d}w\, \mathrm{d}v. \tag{31}$$

By applying the inverse cdf $F_{\mathrm{MK}}^{-1}$ and changing variables to $r = w/v$, we obtain (28). ■

*3) Amorphous Type 2:*

**Theorem 3.** *In $A_2$, when $m_0 = 1$ and $h_1 \sim \Gamma(m, m)$, the SF MD is given by*

$$\bar{F}(t,u) = \int_0^\infty \int_0^\infty \mathbf{1}\left(G(w,v;t) > u\right)\, f_{r_0,r_1}(w,v)\,\mathrm{d}w\,\mathrm{d}v, \quad (32)$$

*where*

$$G(w,v;t) = \left(1 + \frac{t^{\ominus}}{m}\left(\frac{w}{v}\right)^{\alpha}\right)^{-m}\left(1 + \frac{t^{\ominus}}{M} w^{\alpha}\mu_X\right)^{-M}, \quad (33)$$

*and $M$ is obtained based on the point process model and fading in $I'$.*

*Proof:* The conditional success probability for $\mathrm{A}_2$ is given by

$$\begin{aligned} P_t^{(2)} &= \mathbb{P}\left(h_0 > t^{\ominus} r_0^{\alpha}(h_1 r_1^{-\alpha} + X)\,\middle|\, r_0, r_1\right) \\ &= \left(1 + \frac{t^{\ominus}}{m}\left(\frac{r_0}{r_1}\right)^{\alpha}\right)^{-m}\left(1 + \frac{t^{\ominus}}{M} r_0^{\alpha}\mu_X\right)^{-M}. \end{aligned} \quad (34)$$

From (2) and (34), (32) can be obtained. ■

*Remarks.*

- For Thm. 3, $M$ needs to be obtained based on the point process and the fading statistics from non-dominant interferers, while for Thm. 2, the fading statistics of the other interferers are irrelevant.
- Thms. 2 and 3 do not require integration over an infinite range, since the indicator functions restrict the effective support.
- Thms. 2 and 3 express the SF MD as an expectation over the joint distribution of $r_0$ and $r_1$, i.e.,

  $$\bar{F}(t,u) = \mathbb{E}_{r_0,r_1}\left(\mathbb{P}(P_t > u \mid r_0, r_1)\right).$$

  With this formulation, the results apply to any point process for which this distribution is known, and they apply to both cellular and bipolar network types, which will be explored in the next two sections. The only distinction between the two types is that in the cellular case, $r_0$ and $r_1$ are dependent, while in the bipolar case, they are independent.
- From Thms. 2 and 3 it follows that $P_t^{(2)} \geq P_t^{(1)}$, i.e., fading in non-dominant interferers is beneficial. This is obtained by comparing (27) and (33) and applying $\log(1+x) \leq x$ for $x > -1$, which yields

  $$\left(1 + \frac{t^{\ominus}}{M} w^{\alpha}\mu_X\right)^{-M} \geq e^{-t^{\ominus} w^{\alpha}\mu_X}. \quad (35)$$

  This is consistent with $m_0 = 1$ and general fading in bipolar network models, where the success probability is [22, p. 105]

  $$p_{\mathrm{s}} = \mathbb{P}(\mathrm{SF} > t) = \exp\Big(-\lambda\pi {t^{\ominus}}^{\delta} r_0^2\, \mathbb{E}(h^{\delta})\Gamma(1-\delta)\Big). \quad (36)$$

  For $m_0 = 1$ and Nakagami-$m$ fading in the interferers' channels,

  $$\frac{\partial p_{\mathrm{s}}}{\partial m} \leq 0, \quad m > 0,$$

  which shows that stronger fading in the interference improves the success probability.

In the next sections, we apply Thms. 2 and 3 to cellular and bipolar networks.

## V. Cellular Networks

### A. System Model

We consider the system model in Subsection IV-A. We focus on networks with nearest-BS association (NBA), where $x_0 = \arg\min_{x\in\Phi}\|x\|$. This is referred to as NBA-$m$ in [18], where $m$ is the Nakagami fading parameter.

### B. Poisson Point Process

**Corollary 2.** *For the PPP under $A_1$, the SF MD is given by* (28) *when $m_0 = m$, and by* (27) *when $m_0 = 1$ with $h_1 \sim \Gamma(m, m)$, where*

$$f_{r_0,r_1}(w,v) = 4\pi^2\lambda^2\, wv\, e^{-\pi\lambda v^2}, \quad 0 \leq w \leq v < \infty. \quad (37)$$

*Proof:* This is a special case of Thm. 2, with the joint pdf for the PPP given in [22, Sec. 2.4.1]. ■

**Corollary 3.** *Under $A_2$, with $m_0 = 1$ and $h_1 \sim \Gamma(m, m)$, the SF MD is given by* (32)*, where $f_{r_0,r_1}$ is given in* (37)*, and*

$$M = \frac{4\pi\lambda(\alpha-1)}{(\alpha-2)^2} m^{\oplus} r_1^2. \quad (38)$$

*Proof:* Follows from Thm. 3, and for the PPP,

$$\begin{aligned} \mathbb{E}[I'^2 \mid r_1] &= \lambda\int_{r_1}^{\infty} \mathbb{E}[h^2]\, v^{-2\alpha} 2\pi v\,\mathrm{d}v \\ &\quad + \lambda^2 \int_{r_1}^{\infty}\int_{r_1}^{\infty} 4\pi^2 \mathbb{E}[h_i]\,\mathbb{E}[h_j]\, v^{1-\alpha}s^{1-\alpha}\,\mathrm{d}v\,\mathrm{d}s \\ &= \frac{\pi\lambda}{(\alpha-1)m^{\oplus}} r_1^{2-2\alpha} + \frac{4\pi^2\lambda^2\, r_1^{2(2-\alpha)}}{(\alpha-2)^2}, \end{aligned} \quad (39)$$

and $\mathbb{E}(I' \mid r_1) = \mu_{X_1}$. Thus, the variance of $I'$ is obtained as

$$\mathrm{Var}\left[I' \mid r_1\right] = \frac{\pi\lambda}{\alpha-1}\frac{1}{m^{\oplus}} r_1^{2-2\alpha}. \quad (40)$$

Substituting (40) in (23) yields (38). ■

### C. Square Lattice

Let $\Phi$ be a stationary (randomly translated) square lattice with density $\lambda$. The joint cdf of $r_0$ and $r_1$ is provided in (72) to (76), in Appendix E. To apply Thm. 3 to lattice networks, we need the variance of $I'$ to compute $M$. First, we state an important fact about the rigidity of lattices.

**Fact 1.** *In lattices, given the distances to the first and second nearest points, the distances to all other lattice points are deterministic.*

This holds because the reference point must lie at one of two intersection points of the circles centered at the first and second nearest lattice points, and the distances from each intersection point to all other lattice points are identical for both positions due to the symmetry of the lattice.

From Fact. 1, it follows that, given $r_0$ and $r_1$, the only source of randomness in $I'$ is the fading. Thus,

$$\mathrm{Var}(X \mid r_0, r_1) = \mathrm{Var}\Big( \sum_{i\in\mathbb{N}\setminus\{1\}} h_i\, r_i^{-\alpha} \,\Big|\, r_0, r_1\Big) = \frac{1}{m} \sum_{i\in\mathbb{N}\setminus\{1\}} r_i^{-2\alpha}. \quad (41)$$

To compute (41), we define $S_\nu \triangleq \sum_{i\in\mathbb{N}\setminus\{1\}} r_i^{-\nu}$ and

$$S_\nu^N \triangleq \sum_{m,n=-N}^{N} \big[(m-x)^2 + (n-y)^2\big]^{-\nu/2} - r_0^{-\nu} - r_1^{-\nu}, \quad (42)$$

such that

$$\lim_{N\to\infty} S_\nu^N = S_\nu,$$

where $2N$ is the size of the lattice. To compute $S_{2\alpha}$, we utilize the Crandall representation [23, Thm. 2.11], which for a square lattice is defined as

$$Z_\nu^N \triangleq \frac{1}{\Gamma(\nu/2)} \sum_{m,n=-N}^{N} \Big[ G_\nu\Big(\sqrt{(m-x)^2+(n-y)^2}\Big) + G_{2-\nu}\Big(\sqrt{m^2+n^2}\Big)\cos\big(2\pi(mx+ny)\big)\Big], \quad (43)$$

where

$$G_\nu(r) \triangleq \frac{\Gamma\big(\frac{\nu}{2}, \pi r^2\big)}{(\pi r^2)^{\nu/2}},$$

is the Crandall function [23, Def. 2.8]. Hence,

$$\lim_{N\to\infty} Z_\nu^N - r_0^{-\nu} - r_1^{-\nu} = S_\nu.$$

To validate the effectiveness of the Crandall representation compared to direct summation in (42), we compute $S_4^{1000}$ for $\nu = 4$, $N = 1000$, and consider it as the ground truth for $S_4$. The Crandall representation is then evaluated for $\nu = 4$, starting from $N = 1$ and incrementing $N$ until one of the following two conditions is satisfied:

1) $|Z_4^N - S_4^{1000}| < \varepsilon$,
2) $Z_4^N > S_4^{1000}$.

The second condition is included because, in cases where the Crandall series exceeds the target value, increasing $N$ only leads to a further increase in $Z_4^N$, and as a result, the first condition is never satisfied. The results show that for all pairs of $r_0$ and $r_1$, and with $\varepsilon = 0.001$, the required value of $N$ is at most 2, with an average of $N = 1.24$. This confirms that the Crandall series converges rapidly and is significantly more efficient than direct summation. Hence, in the lattices, to obtain more accurate results, the mean interference beyond the nearest interferer is computed using the Crandell series, given by

$$\mu_X = \mu'_X \triangleq Z_\alpha^N.$$

In Fig. 4, we observe $\mu'_X = Z_4^{10}$ for the square lattice with unit density. The figure shows that $\mu'_X$ is primarily influenced by $r_0$, with the most significant variation occurring for $r_0 > 0.5$. Moreover, for each $r_0$, the corresponding $r_1$ is bounded by $\sqrt{r_0^2 - \sqrt{2}r_0 + \lambda}$, which is the upper boundery of $r_0$ given in (72) and (74), in Appendix E.

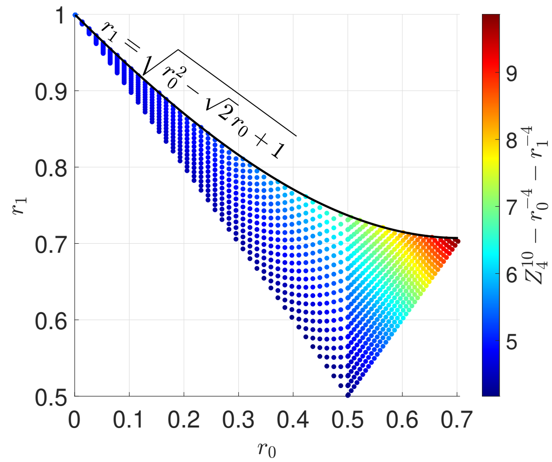


Fig. 4. Visualization of $Z_4^{10} - r_0^{-4} - r_1^{-4}$ for the square lattice with $\lambda = 1$. The colored shape is the support of $f_{r_0,r_1}$, and the black curve shows the maximum $r_1$ for each $r_0$.

**Corollary 4.** *Under A2, when $m_0 = 1$ and $h_1 \sim \Gamma(m, m)$, the SF MD for the square lattice is given by* (32)*, where the joint cdf $F_{r_0,r_1}$ is given in* (72) *to* (76)*, in Appendix E, and $M$ is given by*

$$M = \frac{m\mu'_X}{\sum_{i\in\mathbb{N}\setminus\{1\}} r_i^{-2\alpha}}. \quad (44)$$

*Proof:* Follows from Thm.2, with $M$ obtained by substituting (41) in (23). ■

**Corollary 5.** *For $m_0 = 1$, $h_1 \sim \Gamma(m, m)$, and no fading in non-dominant interferers, A2 reduces to A1. The SF MD is then given by* (27) *in Thm. 2, where $f_{r_0,r_1}$ can be obtained from* (72) *to* (76)*.*

*Proof:* Follows from Thm. 3 and Fact. 1. ■

## D. Numerical Results

A ground truth is required to assess the accuracy of the amorphous models. Although the Gil–Pelaez (GP) theorem provides an exact integral expression for MDs [24], its numerical evaluation requires careful choices of integration limits and step sizes, as discussed in [5]. Moreover, GP relies on the evaluation of moments. While it can be effective in a few special cases where the moment expressions are simple, these expressions themselves are generally complicated, consisting of nested integrals, and the MDs can be quite sensitive to inaccuracies in the moments [13]. In such cases, Monte Carlo simulation is particularly useful, especially when the path loss exponent $\alpha$ is not close to 2. In addition, robust numerical procedures for evaluating the GP integrals are rarely discussed in the literature, making numerical accuracy difficult to assess. Accordingly, the fully granular model obtained via Monte Carlo simulation is used as the ground truth in this work, and all proposed models are evaluated relative to it, consistent with [15].

The family of amorphous models with all links Nakagami-$m$ fading is evaluated based on simulations in Python for the PPP and the square lattice cellular networks. For the PPP, the

TABLE IV
TERMINOLOGY FOR THE QUALITY OF THE APPROXIMATION

| **Terminology** | perfect | excellent | good | acceptable | mediocre | bad |
|---|---|---|---|---|---|---|
| $d(F_1, F_2) \in$ | [0, 0.004] | [0.004, 0.01] | [0.01, 0.02] | [0.02, 0.04] | [0.04, 0.1] | [0.1, 1] |

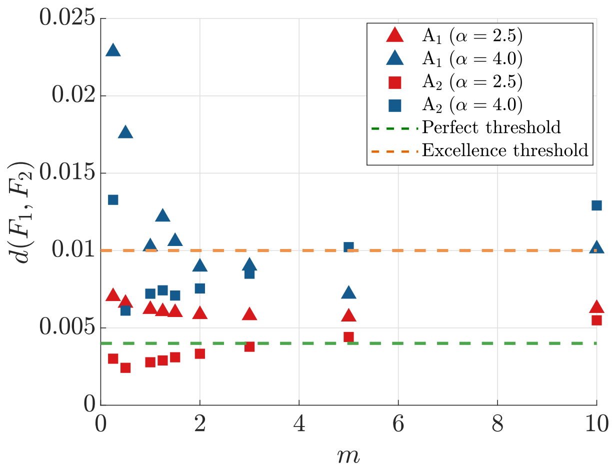


Fig. 5. Total distance vs. $m$ for $A_1$ and $A_2$ in Poisson cellular networks.

TABLE V
RUNTIME SPEED-UP FACTORS OF THE AMORPHOUS MODELS RELATIVE TO THE FULLY GRANULAR MODEL.

| $\alpha$ | $m$ | $A_1$ | $A_2$ |
|---|---|---|---|
| 2.5 | 1.25 | 34.84 | 93.42 |
| | 1.5 | 36.81 | 92.82 |
| | 2 | 75.30 | 75.86 |
| | 3 | 42.97 | 72.34 |
| | 5 | 41.51 | 72.20 |
| | 10 | 40.13 | 72.33 |
| | **Average** | 45.26 | 79.83 |
| 4.0 | 1.25 | 5.41 | 11.99 |
| | 1.5 | 5.83 | 12.00 |
| | 2 | 11.44 | 9.33 |
| | 3 | 5.95 | 9.43 |
| | 5 | 5.89 | 9.22 |
| | 10 | 5.65 | 9.21 |
| | **Average** | 6.70 | 10.19 |

expressions given in (11) and Cor. 2 are used for $A_0$ and $A_1$, respectively. Under Rayleigh fading, Cor. 3 and [1, Thm. 2] are employed for $A_2$ and the fully granular model, respectively. The fully granular model and $A_2$ under general fading for all links are evaluated through Monte Carlo simulations with 5000 fading realizations and 20,000 location realizations. The fading realizations vary per iteration, while the PPP realizations are fixed across iterations. To capture interference accurately, the simulated PPP area for $\alpha = 2.5$ is about 7.5 times larger than for $\alpha = 4$. For $\alpha = 2.5$, the mean interference term in (20) is included, as required when $\alpha < 3$. For the square lattice, all models are evaluated using Monte Carlo simulations. For $A_2$ fading realizations are generated only for the desired link and the dominant interferer. For each user, we compute the success probability and subsequently obtain the ccdf of the success probability for each realization.

We define a distance metric to measure how close two functions are to each other. Let $F_1, F_2 : U \to Y$ be two bounded functions. The total distance between functions $F_1$ and $F_2$ is defined as the $L_1$-norm of $F_1$ and $F_2$ over $U$, i.e., [5]

$$d(F_1, F_2) \triangleq \|F_1 - F_2\|_{L_1(U)} = \int_U |F_1(x) - F_2(x)|\, dx. \quad (45)$$

For SF MDs, we set $U = [0, 1]^2$ and $Y = [0, 1]$, and use the nomenclature in Table IV [5] to assess the quality of an approximation. We utilize (45) to assess the quality of the family of amorphous models in approximating the fully granular model.

Since $A_0$ has a poor match for all values of $\alpha$ and $m$, we focus on the total distance for $A_1$ and $A_2$ in the PPP, along with their speedup factors, as shown in Fig. 5 and Table V, respectively. The speedup factors are obtained by averaging three independent runtime measurements for each model.

$A_1$ shows an excellent match for $\alpha = 2.5$ across all $m$, and for $\alpha = 4$ the match ranges from excellent to good depending on $m$. $A_2$ shows a perfect match for $\alpha = 2.5$ except at $m = 5, 10$, and for $\alpha = 4$, the match is excellent except at $m = 0.25, 5, 10$. For $A_1$, the total distance generally increases as $m$ decreases, indicating reduced accuracy under higher variance since the variability of $\mathring{I}$ is not captured. Conversely, for $A_2$, the total distance generally increases with $m$. In both models, the total distance becomes larger as we approach the no fading and severe fading regimes, suggesting that matching only the first or the first two moments of $\mathring{I}$ is insufficient to accurately capture the MDs in these regimes, particularly for larger $\alpha$. Except at $m = 5, 10$ for $\alpha = 4$, $A_2$ yields smaller total distances than $A_1$, making it the most accurate amorphous model overall.

Moreover, these results show a clear ordering in approximation accuracy as the complexity of the amorphous models increases. The transition from $A_0$ to $A_1$ leads to a significant improvement, since $A_0$ yields a poor match, as discussed above. From $A_1$ to $A_2$, the distances in Fig. 5 are generally smaller, although the improvement is less pronounced than that of $A_0$ to $A_1$. Overall, the results indicate that accounting for higher-order moments of $\mathring{I}$ improves the approximation accuracy, while the incremental improvement between successive approximations becomes smaller.

In terms of computational runtime, Table V reports the speedup factors of $A_1$ and $A_2$ relative to the fully granular model for $m > 1$. On average, $A_2$ runs about $1.5\times$ faster than $A_1$, indicating that the integral in (28) is computationally expensive, although it reduces noise arising from simulating fading and point processes. We also observe that $A_2$, even when implemented via Monte Carlo simulation, is much faster than the fully granular model, particularly as $\alpha$ decreases toward 2. For $m = 1$, the MD is obtained from simpler expressions, resulting in much larger speedup factors. In this

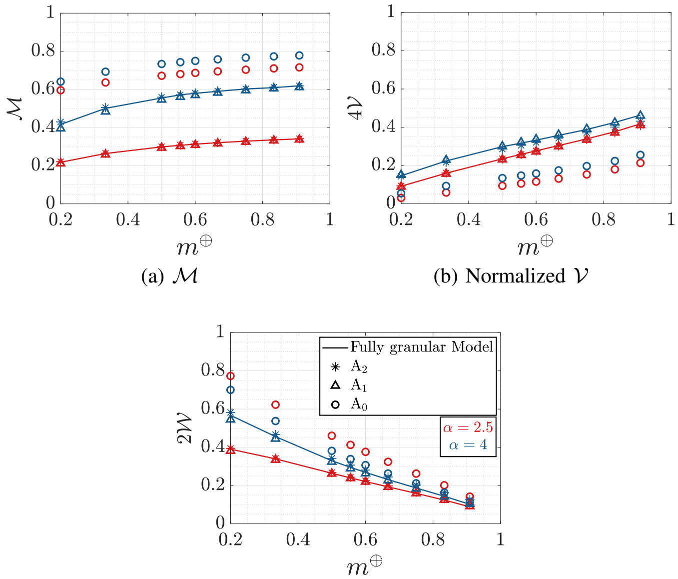


(a) $\mathcal{M}$

(b) Normalized $\mathcal{V}$

(c) Normalized $\mathcal{W}$

Fig. 6. SF MD statistics for the Poisson cellular networks as a function of $m^{\oplus}$, comparing amorphous models with the fully granular model. Red markers denote for $\alpha = 2.5$ and blue markers denote $\alpha = 4$.

TABLE VI

META STATISTICS RELATIVE ERRORS FOR $A_1$ IN POISSON CELLULAR NETWORKS.

| $m$ | $\alpha = 2.5$ | | | $\alpha = 4.0$ | | |
|---|---|---|---|---|---|---|
| | $\mathcal{M}$ | $4\mathcal{V}$ | $2\mathcal{W}$ | $\mathcal{M}$ | $4\mathcal{V}$ | $2\mathcal{W}$ |
| 0.25 | 0.0066 | 0.0027 | 0.0092 | 0.0215 | 0.0047 | 0.0225 |
| 0.5 | 0.0058 | 0.0034 | 0.0054 | 0.0172 | 0.0048 | 0.0115 |
| 1 | 0.0050 | 0.0039 | 0.0025 | 0.0090 | 0.0020 | 0.0057 |
| 1.25 | 0.0047 | 0.0041 | 0.0019 | 0.0113 | 0.0046 | 0.0058 |
| 1.5 | 0.0045 | 0.0041 | 0.0015 | 0.0099 | 0.0049 | 0.0055 |
| 2 | 0.0037 | 0.0035 | 0.0017 | 0.0091 | 0.0044 | 0.0049 |
| 3 | 0.0037 | 0.0026 | 0.0027 | 0.0106 | 0.0038 | 0.0040 |
| 5 | 0.0036 | 0.0012 | 0.0038 | 0.0102 | 0.0028 | 0.0035 |
| 10 | 0.0012 | 0.0026 | 0.0021 | 0.0104 | 0.0042 | 0.0023 |

TABLE VII

META STATISTICS RELATIVE ERRORS FOR $A_2$ IN POISSON CELLULAR NETWORKS.

| $m$ | $\alpha = 2.5$ | | | $\alpha = 4.0$ | | |
|---|---|---|---|---|---|---|
| | $\mathcal{M}$ | $4\mathcal{V}$ | $2\mathcal{W}$ | $\mathcal{M}$ | $4\mathcal{V}$ | $2\mathcal{W}$ |
| 0.25 | 0.0030 | 0.0020 | 0.0041 | 0.0133 | 0.0029 | 0.0150 |
| 0.5 | 0.0018 | 0.0014 | 0.0030 | 0.0041 | 0.0069 | 0.0106 |
| 1 | 0.0014 | 0.0004 | 0.0037 | 0.0044 | 0.0130 | 0.0124 |
| 1.25 | 0.0014 | 0.0001 | 0.0041 | 0.0004 | 0.0114 | 0.0120 |
| 1.5 | 0.0013 | 0.0005 | 0.0045 | 0.0008 | 0.0118 | 0.0123 |
| 2 | 0.0015 | 0.0014 | 0.0038 | 0.0005 | 0.0098 | 0.0126 |
| 3 | 0.0016 | 0.0022 | 0.0025 | 0.0008 | 0.0068 | 0.0100 |
| 5 | 0.0013 | 0.0035 | 0.0009 | 0.0004 | 0.0060 | 0.0065 |
| 10 | 0.0011 | 0.0045 | 0.0010 | 0.0007 | 0.0032 | 0.0032 |

case, $A_1$ achieves speedups of 189.80 and 26.96 for $\alpha = 2.5$ and $\alpha = 4$, respectively, and $A_2$ yields corresponding speedups of 163.88 and 22.69. Thus, $A_1$ is slightly faster than $A_2$, and both are considerably faster than the fully granular model, highlighting the value of Cors. 2 and 3.

From Fig. 6a to Fig. 6c, we observe normalized values of $\mathcal{M}$, $\mathcal{V}$, and $\mathcal{W}$, respectively, for the Poisson cellular network model, where $\mathcal{V}$ is multiplied by 4 and $\mathcal{W}$ by 2 so that all meta statistics are within $[0, 1]$, providing a unified basis for comparison and interpretation. The corresponding relative errors of the meta statistics for $A_1$ and $A_2$ are given in Tables VI and VII, respectively. In general, we observe that $A_0$ deviates significantly from the fully granular model. However, as previously mentioned, it remains valuable due to its advantages. We also observe that as $\alpha$ increases, the gaps between $A_0$ and $A_1$, as well as $A_2$ decrease. This is because, as $\alpha$ increases, the interference from distant BSs becomes less significant. Conversely, as $\alpha$ decreases to 2, the gaps increase as the distant BSs have greater influence on the interference. General observations from the figures and tables for $A_1$ and $A_2$ are as follows: meta statistics are approximated more accurately for lower $\alpha$ values, consistent with the earlier discussion. $A_2$ provides a better approximation of $\mathcal{M}$ than $A_1$. For $\alpha = 2.5$, $\mathcal{V}$ and $\mathcal{W}$ are, in most cases, better captured by $A_2$ than $A_1$, whereas for $\alpha = 4$ the opposite holds.

The SF MD statistics for the square lattice are shown in Fig. 7. We observe that the results for $A_1$ and $A_2$ are very close, suggesting that the variance of $I'$ is negligible in this case. Interestingly, $\mathcal{V}$ exhibits a non-monotonic relation with $\alpha$, in contrast to the monotonic trend observed under the PPP.

By comparison of both the SF MD statistics and the total distances, we conclude that $A_2$ is the most accurate amorphous model. Moreover, comparing the meta statistics can provide deeper insights into the aspects in which an approximation may differ from the granular model. For instance, if the error in $\mathcal{W}$ is high, we can infer that the discrepancy arises from the impact of fading.

While the numerical results provide insight into the accuracy of the amorphous models, a theoretical characterization of the approximation error would be valuable but remains challenging. This is because the contribution of interferers beyond the nearest one depends strongly on their random spatial locations; in particular, these interferers may cluster near the nearest interferer or be located much farther away, leading to significant variability in the residual interference. This effect is especially important for $A_2$. In principle, Markov and Chebyshev inequalities could be applied to $A_1$ and $A_2$, respectively, but the resulting bounds cannot be expected to be tight.

### E. SF MD with General Propagation Effects

The method of amorphous modeling extends to general network models with a variety of propagation effects. To show this, we employ the path loss point process (PLP), defined as

$$\Xi \triangleq \left\{ \frac{\|x\|^{\alpha}}{V_x} : x \in \Phi \right\} \subset \mathbb{R}^{+}, \tag{46}$$

where $V_x$ are iid with $\mathbb{E}[V^{\delta}] < \infty$ [18], [25], representing large-scale propagation effects such as shadowing, line-of-sight (LOS) and non-line-of-sight (NLOS) conditions, or antenna directionality. Under maximum-average-received-power association, the desired transmitter and dominant interferer are given by

$$x_0 = \arg\min_{x \in \Phi} \frac{\|x\|^{\alpha}}{V_x}, \qquad x_1 = \arg\min_{x \in \Phi \setminus \{x_0\}} \frac{\|x\|^{\alpha}}{V_x},$$

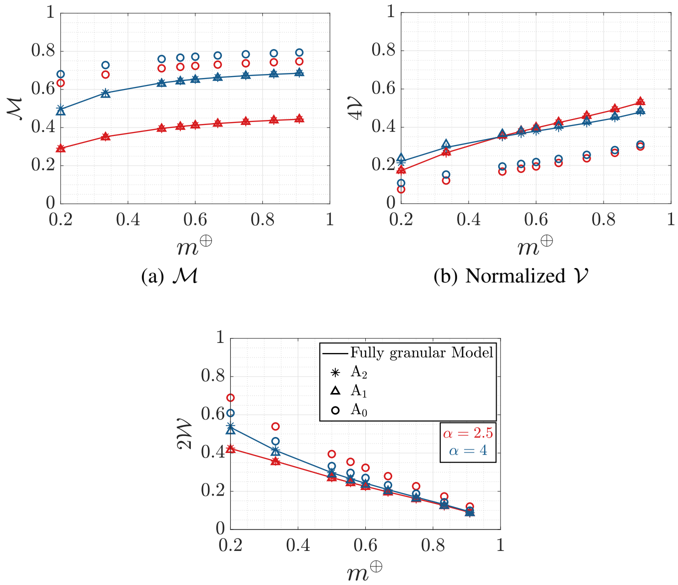


(a) $\mathcal{M}$

(b) Normalized $\mathcal{V}$

(c) Normalized $\mathcal{W}$

Fig. 7. SF MD statistics for square lattice cellular networks as a function of $m^{\oplus}$, comparing amorphous models with the fully granular model. Red markers denote $\alpha = 2.5$ and blue markers denote $\alpha = 4$.

respectively. Let $\Xi = \{\xi_0, \xi_1, \xi_2, \dots\}$ be the elements of the PLP, ordered increasingly. The desired signal, dominant interference, and residual interference are given by

$$S = \frac{h_0}{\xi_0}, \qquad I_{\mathrm{D}} = \frac{h_1}{\xi_1}, \qquad I' = \sum_{i \geq 2} \frac{h_i}{\xi_i}.$$

Substituting the above expressions into (24) yields the SF, which now incorporates large-scale propagation effects through the PLP. Under amorphous models, the $\mathrm{SF}_k$ follow from (25), where

$$\mu_X \triangleq \mathbb{E}\left[I' \mid \xi_1\right] = \lambda\pi\,\mathbb{E}\left[V^{\delta}\right] \delta^{\ominus} \xi_1^{\delta-1},$$

and

$$M \triangleq \frac{1}{\mathrm{Var}(H \mid \xi_0, \xi_1)} = \frac{\mu_X^2}{\mathrm{Var}(X \mid \xi_0, \xi_1)}.$$

The corresponding SF MD is then given by

$$\bar{F}(t, u) = \mathbb{P}\Big(P_t^{(k)} > u\Big),$$

where

$$P_t^{(k)} \triangleq \mathbb{P}(\mathrm{SF}_k > t \mid \xi_0, \xi_1).$$

In the case of a PPP, the analysis based on the PLP is straightforward, since the PLP is itself Poisson with intensity measure $\Lambda([0, r]) = \lambda\pi\mathbb{E}[V^{\delta}]\, r^{\delta}$ [25].

## VI. Bipolar Networks

### A. System Model

We consider the system model in Subsection IV-A, where the set of interferers $\Phi'$ forms a stationary point process. Each transmitter has an associated receiver at a distance $r_0$ in a random orientation [22, Def, 5.8]. The fading and path loss models are the same as in the cellular case.

In bipolar networks, the joint pdf $f_{r_0, r_1}$ factorizes due to the independence of $r_0$ and $r_1$. If $r_0 = R$ is deterministic,

$$f_{r_0, r_1}(w, v) = \delta(w - R)\, f_{r_1}(v),$$

where $\delta(\cdot)$ is the Dirac delta function. The following corollaries are derived for this case.

### B. Poisson Point Process

Let $\Phi'$ be a PPP. For the PPP [22, Sec. 2.4.1]

$$f_{r_1}(v) = 2\pi\lambda v e^{-\pi\lambda v^2}, \quad v \geq 0. \tag{47}$$

**Corollary 6.** *In $A_2$, with $m_0 = 1$, the SF MD for the PPP is given by*

$$\bar{F}(t, u) = \int_0^{\infty} \mathbf{1}\left\{\left(1 + \frac{t^{\ominus}}{m}\left(\frac{R}{v}\right)^{\alpha}\right)^{-m} \right. \tag{48}$$

$$\left. \left(1 + \frac{t^{\ominus}}{M} R^{\alpha} \mu_X\right)^{-M} > u\right\} 2\pi\lambda v e^{-\pi\lambda v^2}\, \mathrm{d}v, \tag{49}$$

*where, $M$ is given in* (38).

*Proof:* Follows from Thm. 3 and (47). ■

### C. Square Lattice

Let $\Phi'$ be a randomly translated square lattice of density $\lambda$. In this case [26]

$$f_{r_1}(v) = \begin{cases} 2\pi\lambda v, & 0 < v \leq \frac{1}{2\sqrt{\lambda}}, \\ 2\pi\lambda v - 8\lambda v \arccos\left(\frac{1}{2\sqrt{\lambda} v}\right), & \frac{1}{2\sqrt{\lambda}} < v < \frac{1}{\sqrt{2\lambda}}. \end{cases} \tag{50}$$

**Corollary 7.** *In $A_2$, with $m_0 = 1$, the SF MD for the lattice network model is given by*

$$\begin{aligned} \bar{F}(t, u) = &\int_0^{\frac{1}{2\sqrt{\lambda}}} \mathbf{1}\{G(R, v; t) > u\}\, 2\pi\lambda v\, \mathrm{d}v \\ &+ \int_{\frac{1}{2\sqrt{\lambda}}}^{\frac{1}{\sqrt{\lambda}}} \mathbf{1}\{G(R, v; t) > u\} \Bigg[2\pi\lambda v \\ &\qquad - 8\lambda v \arccos\left(\frac{1}{2\sqrt{\lambda} v}\right)\Bigg] \mathrm{d}v, \end{aligned} \tag{51}$$

*where $G(R, v; t)$ is evaluated by obtaining $M$ from $\mathrm{Var}(I' \mid r_1)$ using the law of total variance, substituting into* (23)*, and setting $w = R$ in* (33).

*Proof:* Follows from Thm. 3 and (50). ■

As in the cellular case, general propagation effects can be incorporated by using the PLP (46).

## VII. Conclusion

The widely used methods for approximating MDs rely on MD moments. However, obtaining MD moments is not always straightforward. Moreover, comparing MDs across different networks does not clearly reveal how variations in random elements, such as fading and the point process, contribute to their differences. To address these challenges, meta statistics are introduced, providing comprehensive information about MDs, including the overall network performance and the variability induced by fading and the point process.

For a systematic MD approximation, we introduce the family of amorphous models $A_0$, $A_1$, and $A_2$, ranked by increasing computational cost and accuracy. We suggest using $A_0$ to capture overall trends and asymptotic behavior. $A_1$ is recommended when the randomness of non-dominant interferers is either small or not critical to the analysis. Moreover, $A_1$ can also serve as a lower bound for $A_2$, since we have shown that fading in the interference improves the success probability. $A_2$ provides sufficient accuracy for most practical purposes.

The proposed meta statistics capture the key features of a two-dimensional distribution in three scalar values, analogous to how the mean and variance describe distributions. They separately capture the impact of fading and the point process, as well as the overall performance of the network. Our accuracy analysis, based on the total distances for SF MDs and the relative error for meta statistics, demonstrates that comparisons across different networks can be based on meta statistics alone, without requiring the full MD.

## APPENDIX

### A. Proof of Expressions in Table IIa

For Nakagami fading with a parameter $m$, we consider only the nearest interferer BS. Let $U = h_1/h_2$, where $h_1$ and $h_2$ are iid gamma RVs, and $Y = (r_2/r_1)^\alpha$, where $r_1$ and $r_2$ are the distances to the serving BS and the nearest interfering BS, respectively. For DR, the success probability is

$$\begin{aligned}\bar{G}(t) &= \mathbb{P}(\mathrm{SF} > t) = \mathbb{P}(U > t^{\ominus} y) \\ &= 1 - F_U(t^{\ominus} y) = 1 - I\left(\frac{t^{\ominus}}{\rho}; m, m\right),\end{aligned} \tag{52}$$

where $I(\cdot; m, m)$ is the regularized incomplete beta function and $\rho = (r_2/r_1)^\alpha$ is deterministic. From (2) the MD is derived as follows

$$\bar{F}(t, u) = \mathbf{1}(\bar{G}(t) > u), \tag{53}$$

and from (3) to (6), the moments and scalars can be obtained.

### B. Proof of Expressions in Table IIb

Without fading, we have $h_1 = h_2 = 1$. The conditional success probability is given by

$$\mathbb{P}(\mathrm{SF} > t \mid \Phi) = \mathbb{P}(Y > t^{\ominus} \mid \Phi) \tag{54}$$

$$= \min\left\{1, (t^{\ominus})^{-\delta}\right\} \tag{55}$$

$$= \begin{cases} 1, & \text{if } t < \frac{1}{2}, \\ (t^{\ominus})^{-\delta}, & \text{if } t \geq \frac{1}{2}. \end{cases} \tag{56}$$

Thus, the SF MD and the moments are obtained as

$$\bar{F}(t, u) = \begin{cases} 1, & t < \frac{1}{2}, \\ (t^{\ominus})^{-\delta}, & t \geq \frac{1}{2}. \end{cases} \tag{57}$$

$$M_b^{\mathrm{RD}}(t) = \begin{cases} 1, & \text{if } t < \frac{1}{2}, \\ (t^{\ominus})^{-\delta}, & \text{if } t \geq \frac{1}{2}. \end{cases} \tag{58}$$

The $\mathcal{V}$ is given by

$$\mathcal{V}^{\mathrm{RD}} = \int_{\frac{1}{2}}^{1} \left((t^{\ominus})^{-\delta} - (t^{\ominus})^{-2\delta}\right) \mathrm{d}t \tag{59}$$

$$\begin{aligned}&= \left[B(1-\delta, \delta+1) - B_{\frac{1}{2}}(1-\delta, \delta+1)\right] \\ &\quad - \left[B(1-2\delta, 2\delta+1) - B_{\frac{1}{2}}(1-2\delta, 2\delta+1)\right].\end{aligned} \tag{60}$$

Since

$$\Gamma(1-\delta)\Gamma(\delta+1) \equiv \frac{\pi\delta}{\sin(\pi\delta)},$$

we have

$$\mathcal{V}^{\mathrm{RD}} = \frac{1}{\mathrm{sinc}(\delta)} - \frac{1}{\mathrm{sinc}(2\delta)} - C, \quad \delta \in (0,1) \setminus \{\frac{1}{2}\},$$

where,

$$C = B_{\frac{1}{2}}(1-\delta, \delta+1) - B_{\frac{1}{2}}(1-2\delta, 2\delta+1).$$

### C. Proof of Expressions in Table IIc

For the deterministic transceivers placement with no fading, the success probability $\bar{G}(t)$ simplifies to

$$\bar{G}(t) = \begin{cases} 1, & \text{if } t < \rho^{\oplus}, \\ 0, & \text{if } t \geq \rho^{\oplus}. \end{cases} \tag{61}$$

The SF MD is derived as

$$\bar{F}(t, u) = \begin{cases} 1, & \text{if } t < \rho^{\oplus}, \\ 0, & \text{otherwise}, \end{cases} \tag{62}$$

and from (3) to (6), the moments and scalars can be obtained.

### D. Proof of Lemma 1

In $A_1$, for $m_0 = m$, let

$$G = h_0 - t^{\ominus} h_1 R^\alpha, \tag{63}$$

where $R = r_0/r_1$, the conditional success probability can be expressed as

$$P_t = \mathbb{P}(G > \kappa R^\alpha r_1^2 \mid r_0, r_1), \tag{64}$$

where $\kappa$ is defined as

$$\kappa \triangleq \frac{2\pi\lambda t^{\ominus}}{\alpha - 2}. \tag{65}$$

For Nakagami fading, $G$ is the difference between two independent gamma RVs.

Generally, if $X_1 \sim \mathcal{G}(m, \beta_1)$ and $X_2 \sim \mathcal{G}(m, \beta_2)$, their difference $Y = X_1 - X_2$ follows a McKay Type II distribution. The pdf of $Y$ is given by [21].

$$f_Y(y) = \begin{cases} \frac{(1-c^2)^{a+\frac{1}{2}} |y|^a}{\sqrt{\pi} 2^a b^{a+1} \Gamma(a+\frac{1}{2})} e^{-\frac{cy}{b}} K_a(\frac{|y|}{b}), & y \neq 0, \\ \frac{(1-c^2)^{a+\frac{1}{2}} \Gamma(a)}{\sqrt{\pi} 2b \Gamma(a+\frac{1}{2})}, & y = 0, \end{cases} \tag{66}$$

where $a > -\frac{1}{2}$, $b > 0$, and $|c| < 1$, with the parameters defined as

$$a = m - \frac{1}{2}, \quad b = \frac{2\beta_1\beta_2}{\beta_1 + \beta_2}, \quad c = -\frac{\beta_1 - \beta_2}{\beta_1 + \beta_2}.$$

Here, $K_a(\cdot)$ denotes the modified Bessel function of the second kind.

$G$ can be expressed as

$$G = X_1 - X_2,$$

where

$$X_1 = h_0, \quad X_2 = t^{\ominus} h_1 R^{\alpha}.$$

Here, $X_1$ and $X_2$ are independent RVs distributed as

$$X_1 \sim \mathcal{G}\left(m, \beta_1 = \frac{1}{m}\right), \quad X_2 \sim \mathcal{G}(m, \beta_2 = \frac{t^{\ominus}}{m} R^{\alpha}).$$

Thus, the Type II McKay distribution can be utilized, where the parameters $b$ and $c$ are given by

$$\begin{aligned} b &= \frac{2}{m}(t^{\ominus} R^{\alpha})^{\oplus}, \\ c &= 2(t^{\ominus} R^{\alpha})^{\oplus} - 1, \end{aligned}$$

conditioned on $R$. So, the conditional success probability in (64) can be expressed using the cdf of the McKay Type II distribution $F_Y$, as

$$p = 1 - F_Y(\kappa R^{\alpha} r_1^2). \tag{67}$$

For Rayleigh fading, where $m_0 = m = 1$, we have $a = 1/2$. In this case, the cdf of the McKay distribution is given by

$$F_Y(y) = \begin{cases} \frac{1+c}{2} e^{(1-c)y/b}, & y < 0, \\ 1 - \frac{1-c}{2} e^{-(1+c)y/b}, & y \geq 0, \end{cases} \tag{68}$$

and the conditional success probability in (64) is expressed by (68) for $y \geq 0$, since $\tau > 0$. The parameters are obtained as

$$\beta_1 = 1, \quad \beta_2 = t^{\ominus} R^{\alpha}, \tag{69}$$

$$c = 2(t^{\ominus} R^{\alpha})^{\oplus} - 1, \tag{70}$$

$$b = 2(t^{\ominus} R^{\alpha})^{\oplus}, \tag{71}$$

and (64) is expressed as

$$P_t = (t^{\ominus} R^{\alpha})^{\oplus} e^{-\frac{2\pi\lambda}{\alpha-2} R^{\alpha} r_1^2}.$$

### E. Distribution of Distances to the two Nearest Neighbors

The following is the piecewise cdf of the distances to the first and second nearest points in a square lattice, as derived in [27, Sec. 2.1].

(i) $0 < w \leq \frac{1}{2\sqrt{\lambda}}, \ \frac{1}{\sqrt{\lambda}} - w < v \leq \sqrt{w^2 - \sqrt{\frac{2}{\lambda}} w + \frac{1}{\lambda}}$,

$$\begin{aligned} F(w,v) &= 4\lambda w^2 \arccos\left(\frac{\lambda(w^2 - v^2) + 1}{2\sqrt{\lambda} w}\right) \\ &\quad + 4\lambda v^2 \arccos\left(\frac{\lambda(v^2 - w^2) + 1}{2\sqrt{\lambda} v}\right) \\ &\quad - 2\sqrt{4\lambda w^2 - \{\lambda(w^2 - v^2) + 1\}^2}. \end{aligned} \tag{72}$$

(ii) $0 < w \leq \frac{1}{2\sqrt{\lambda}}, \ \sqrt{w^2 - \sqrt{\frac{2}{\lambda}} w + \frac{1}{\lambda}} < v \leq \frac{1}{\sqrt{\lambda}}$,

$$\begin{aligned} F(w,v) &= \lambda\pi w^2 + 4\lambda v^2 \left(\arcsin\left(\frac{1}{\sqrt{2\lambda} v}\right) - \frac{\pi}{4}\right) \\ &\quad - 4\sqrt{\lambda} v \sin\left(\arcsin\left(\frac{1}{\sqrt{2\lambda} v}\right) - \frac{\pi}{4}\right). \end{aligned} \tag{73}$$

(iii)

$$\frac{1}{2\sqrt{\lambda}} < w \leq \frac{1}{\sqrt{2\lambda}}, \ w < v \leq \sqrt{w^2 - \sqrt{\frac{2}{\lambda}} w + \frac{1}{\lambda}}, \tag{74}$$

$$\begin{aligned} F(w,v) &= 4\lambda w^2 \arccos\left(\frac{\lambda(w^2 - v^2) + 1}{2\sqrt{\lambda} w}\right) \\ &\quad - 4\lambda \ w^2 \arccos\left(\frac{1}{2\sqrt{\lambda} w}\right) \\ &\quad + 4\lambda v^2 \arccos\left(\frac{\lambda(v^2 - w^2) + 1}{2\sqrt{\lambda} v}\right) \\ &\quad + \sqrt{4\lambda w^2 - 1} - 2\sqrt{4\lambda w^2 - \lambda(w^2 - v^2) + 1\}^2}. \end{aligned} \tag{75}$$

(iv) $\frac{1}{2\sqrt{\lambda}} < w \leq \frac{1}{\sqrt{2\lambda}}, \ \sqrt{w^2 - \sqrt{\frac{2}{\lambda}} w + \frac{1}{\lambda}} < v \leq \frac{1}{\sqrt{\lambda}}$,

$$\begin{aligned} F(w,v) &= \lambda\pi w^2 - 4\lambda w^2 \arccos\left(\frac{1}{2\sqrt{\lambda} w}\right) \\ &\quad + 4\lambda v^2 \left(\arcsin\left(\frac{1}{\sqrt{2\lambda} v}\right) - \frac{\pi}{4}\right) \\ &\quad - 4\sqrt{\lambda} v \sin\left(\arcsin\left(\frac{1}{\sqrt{2\lambda} v}\right) - \frac{\pi}{4}\right) \\ &\quad + \sqrt{4\lambda w^2 - 1}. \end{aligned} \tag{76}$$

## References


[1] M. Haenggi, “The meta distribution of the SIR in Poisson bipolar and cellular networks,” *IEEE Transactions on Wireless Communications*, vol. 15, no. 4, pp. 2577–2589, 2016.

[2] ——, “Meta distributions—part 1: Definition and examples,” *IEEE Communications Letters*, vol. 25, no. 7, pp. 2089–2093, 2021.

[3] ——, “Meta distributions—part 2: Properties and interpretations,” *IEEE Communications Letters*, vol. 25, no. 7, pp. 2094–2098, 2021.

[4] X. Wang and M. Haenggi, “Hausdorff moment transforms and their performance,” *Probability in the Engineering and Informational Sciences*, pp. 1–26, 2025.

[5] ——, “Fast Hausdorff moment transforms for meta distributions in wireless networks,” *IEEE Transactions on Wireless Communications*, vol. 23, no. 4, pp. 2607–2621, 2024.

[6] S. Guruacharya and E. Hossain, “Approximation of meta distribution and its moments for Poisson cellular networks,” *IEEE Wireless Communications Letters*, vol. 7, no. 6, pp. 1074–1077, 2018.

[7] M. Haenggi, “Efficient calculation of meta distributions and the performance of user percentiles,” *IEEE Wireless Communications Letters*, vol. 7, no. 6, pp. 982–985, 2018.

[8] Y. Sun, Q. Liu, and H. Wang, “SIR meta distribution in the heterogeneous and hybrid networks,” *Wireless Communications and Mobile Computing*, vol. 2020, no. 1, p. 8856459, 2020.

[9] L. Yang, F.-C. Zheng, Y. Zhong, and S. Jin, “Spatio-temporal analysis of meta distribution for cell-center/cell-edge users,” *IEEE Transactions on Communications*, vol. 69, no. 12, pp. 8256–8270, 2021.

[10] S. Wang and M. Di Renzo, “On the meta distribution in spatially correlated non-Poisson cellular networks,” *EURASIP Journal on Wireless Communications and Networking*, vol. 2019, pp. 1–11, 2019.

[11] C. Saha, M. Afshang, and H. S. Dhillon, “Meta distribution of downlink SIR in a Poisson cluster process-based HetNet model,” *IEEE Wireless Communications Letters*, vol. 9, no. 12, pp. 2144–2148, 2020.

[12] P. Madhusudhanan, J. G. Restrepo, Y. Liu, and T. X. Brown, “Analysis of downlink connectivity models in a heterogeneous cellular network via stochastic geometry,” *IEEE Transactions on Wireless Communications*, vol. 15, no. 6, pp. 3895–3907, 2016.

[13] X. Wang and M. Haenggi, “The sensitivity of meta distributions to their moments,” *IEEE Transactions on Wireless Communications*, vol. 23, no. 12, pp. 19 003–19 016, 2024.

[14] M. Haenggi, “Simalysis: Symbiosis of simulation and analysis,” Oct. 2020, accessed: Feb. 3, 2025. [Online]. Available: https://stogblog.net/2020/10/15/simalysis-symbiosis-of-simulation-and-analysis/
[15] Y. Qin, M. A. Kishk, and M.-S. Alouini, “A dominant interferer plus mean field-based approximation for SINR meta distribution in wireless networks,” *IEEE Transactions on Communications*, vol. 71, no. 6, pp. 3663–3678, 2023.
[16] M. Shi, X. Gao, H. Yuan, D. Niyato, and K. Yang, “Spatial outage capacity analysis in Poisson networks with dynamic traffic,” *IEEE Transactions on Communications*, vol. 73, no. 10, pp. 9119–9133, 2025.
[17] V. V. Chetlur and H. S. Dhillon, “Downlink coverage analysis for a finite 3-d wireless network of unmanned aerial vehicles,” *IEEE Transactions on Communications*, vol. 65, no. 10, pp. 4543–4558, 2017.
[18] M. Haenggi, “SIR analysis via signal fractions,” *IEEE Communications Letters*, vol. 24, no. 7, pp. 1358–1362, 2020.
[19] K. Feng and M. Haenggi, “The SINR meta distribution in Poisson cellular networks,” *IEEE Wireless Communications Letters*, vol. 10, no. 7, pp. 1385–1389, 2021.
[20] M. Haenggi, “Q cells in wireless networks,” *IEEE Transactions on Wireless Communications*, vol. 25, pp. 9719–9730, 2026.
[21] H. Holm and M.-S. Alouini, “Sum and difference of two squared correlated Nakagami variates in connection with the McKay distribution,” *IEEE Transactions on Communications*, vol. 52, no. 8, pp. 1367–1376, 2004.
[22] M. Haenggi, *Stochastic Geometry for Wireless Networks*. Cambridge University Press, 2012.
[23] A. A. Buchheit, J. Busse, and R. Gutendorf, “Computation and properties of the Epstein zeta function with high-performance implementation in epsteinlib,” 2024. [Online]. Available: https://arxiv.org/abs/2412.16317
[24] J. Gil-Pelaez, “Note on the inversion theorem,” *Biometrika*, vol. 38, no. 3-4, pp. 481–482, 1951.
[25] X. Zhang and M. Haenggi, “The performance of successive interference cancellation in random wireless networks,” *IEEE Transactions on Information Theory*, vol. 60, no. 10, pp. 6368–6388, 2014.
[26] M. Miyagawa, “Order distance in regular point patterns,” *Geographical Analysis*, vol. 41, no. 3, pp. 252–262, 2009.
[27] ——, “Joint distribution of distances to the first and the second nearest facilities,” *Journal of Geographical Systems*, vol. 14, pp. 209–222, 2012.